Engineering Structures 37 (2012) 106–124

Contents lists available at SciVerse ScienceDirect

Engineering Structures

journal homepage: www.elsevier.com/locate/engstruct

Topology optimization for braced frames: Combining continuum and beam/column elements

Lauren L. Stromberg [a], Alessandro Beghini [b], William F. Baker [b], Glaucio H. Paulino [a,*]

[a] Department of Civil and Environmental Engineering, University of Illinois at Urbana-Champaign, Newmark Laboratory, 205 N. Mathews Avenue, Urbana, IL 61801, USA
[b] Skidmore, Owings & Merrill, LLP, 224 S. Michigan Avenue, Chicago, IL 60604, USA

ARTICLE INFO

Article history:
Received 15 April 2011
Revised 13 December 2011
Accepted 14 December 2011

Keywords:
Topology optimization
High-rise buildings
Material layout
Braced frames
Lateral systems
Continuum and discrete elements
Optimal braced frame geometry

ABSTRACT

This paper describes an integrated topology optimization technique with concurrent use of both continuum four-node quadrilateral finite elements and discrete two-node beam elements to design structural braced frames that are part of the lateral system of a high-rise building. The work explores the analytical aspects of optimal geometry for braced frames to understand the underlying behavior and provides a theoretical benchmark to compare numerical results. The influence of the initial assumptions for the interaction between the quadrilaterals and the frame members are discussed. Numerical examples are given to illustrate the present technique on high-rise building structures.

1. Introduction

Topology optimization is common in mechanical and aeronautical engineering, and it has been, in recent years, progressively embraced for structural engineering applications. Examples are the multi-story building design or long span bridge design applications presented in Stromberg et al. [1], Allahdadian and Boroomand [2], Neves et al. [3], or Huang and Xie [4]. Despite a variety of applications within the civil engineering field, the focus of this work is towards high-rise buildings, where engineers are faced with the challenge of identifying the optimal topology of the lateral bracing system that minimizes material usage and corresponding cost. Therefore, the scope of this work is to introduce a methodology using topology optimization for isotropic, homogeneous material that enables engineers to develop the lateral system from the conceptual optimal bracing angles to the final sizing of the members.

The methodology presented in Stromberg et al. [1] represents an initial attempt at identifying optimal bracing angles. However, it presents some limitations as illustrated in the problem of Fig. 1, which shows a schematic for a high-rise building subject to wind loading. The previous work (see Fig. 1b) was limited due to high concentrations of material towards the edges of the domain, consistent with the flange versus web behavior, described in Section 4 of Stromberg et al. [1]. Such concentrations impede the identification of the working points of the column to the diagonal intersections. In addition, the columns are so wide that they possess high flexural stiffness. In practice, this is not realistic because the columns are relatively narrow compared to the width of the building. Moreover, since the continuum topology optimization problem has a constraint on the volume fraction and a large amount of material forms the column members, a relatively low volume is available for the diagonals. As a result, there is an incomplete diagonalization in the frame (i.e. missing diagonals at the base of the frame). Thus, one would have to introduce an additional constraint to distribute material between the columns and the diagonals to prevent concentrations at the edges.

This paper introduces a combination of discrete (beam/column) members and continuum quadrilateral members to overcome the aforementioned issues. In Fig. 1c and d, six discrete (truss) members are added to model each column while maintaining the same total volume of material as the problem in Fig. 1b. As a result, the concentration of material at the edges is eliminated, and a complete diagonalization with clear working points emerges.

1.1. Motivation for braced structural systems

Braced frame and moment frame structural systems are commonly deployed in the lateral design of high-rise buildings. Braced

* Corresponding author. Tel.: +1 333 3817; fax: +1 217 2658041.
E-mail addresses: paulino@illinois.edu, paulino@uiuc.edu (G.H. Paulino).

0141-0296/$ - see front matter © 2011 Elsevier Ltd. All rights reserved.
doi:10.1016/j.engstruct.2011.12.034

Nomenclature

A_0	cross-sectional area of column sized for constant stress	r_{min}	minimum radius of projection
A_i	cross-sectional area of member i	$\mathbf{u}$	global displacement vector
B	half the width of a frame	u_i	horizontal displacement of node i
c	compliance of the design	v_i	vertical displacement of node i
$\mathbf{E}$	Young's modulus computed through SIMP	V	total volume
E_0	Young's modulus of solid material	V_s	maximum volume constraint
E_i	Young's modulus of member i	W_{ext}	external work of a frame
$\mathbf{f}$	global load vector	W_{int}	internal work of a frame
F_i	internal force in member i from real system	$\mathbf{x}$	a point in the design domain
f_i	internal force in member i from virtual system	x_i	x-coordinate of node i
H	overall height of a frame	y_i	y-coordinate of node i
I	moment of inertia	z_i	height of the i^{th} bracing intersection point
k	proportionality constant	Δ	deflection
$\mathbf{K}$	global stiffness matrix	Δ_{req}	target or allowable deflection
L_i	length of member i	ϵ	strain
m	number of diagonal members	θ_i	pseudo-rotation at node i
n	index of module in a frame	λ	Lagrange multiplier
N	total number of modules	ν	Poisson's ratio
p	penalization factor for SIMP	ρ	density
P_i	point load at point i	σ_i	stress in member i
		Ω	design domain

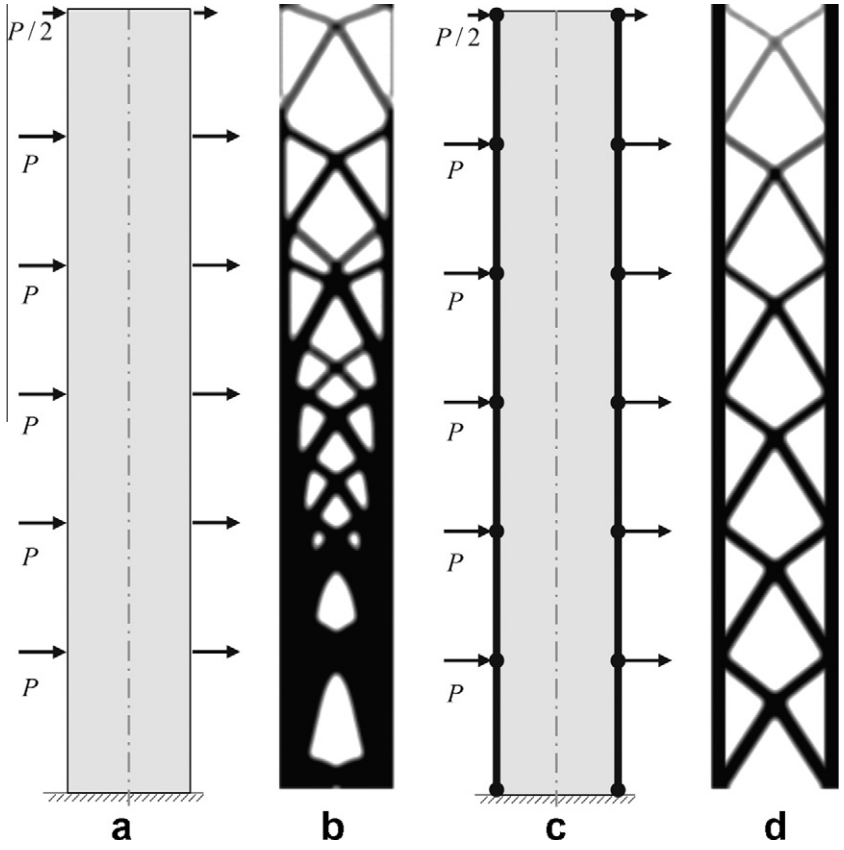

Fig. 1. Comparison of existing topology optimization techniques with technique proposed in this work considering the same total volume of material: (a) problem statement for continuum approach, (b) topology optimization result using quadrilateral elements, (c) problem statement for combined approach, and (d) topology optimization result with quadrilateral and discrete "column" elements.

frames have been used in several noteworthy buildings like the John Hancock Center (Chicago, IL), Broadgate Tower (London, UK) and Bank of China Tower (Hong Kong), as shown in Fig. 2. The design of such systems is traditionally based on diagonal braces arranged according to a 45° or 60° angle and variations in-between these two angles. However, there have been few engineering studies in the past to identify the optimal bracing angle and the parameters affecting such angles [5]. The scope of this paper consists of exploring optimal bracing layouts to maximize structural performance while minimizing material. Various measures of structural

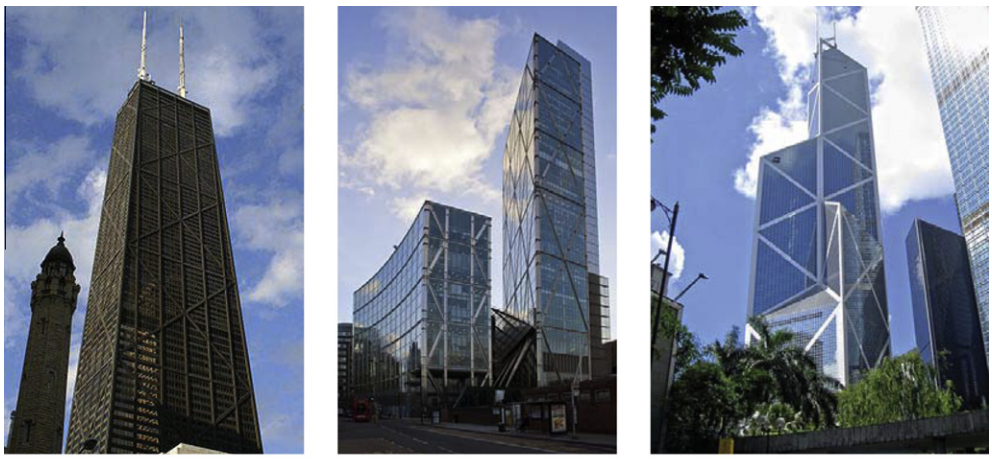

Fig. 2. Existing buildings featuring remarkable braced frame systems: (a) John Hancock Center in Chicago, IL (http://en.wikipedia.org/wiki/John_Hancock_Center), (b) Broadgate Tower in London, UK (http://en.wikipedia.org/wiki/Broadgate_Tower), and (c) Bank of China Tower in Hong Kong (http://en.wikipedia.org/wiki/Bank_of_China).

performance could include tip displacement, frequency, compliance, critical buckling load, etc. The examples of this paper focus on minimizing the compliance and relating this quantity to building behavior and design.

The utilization of the optimization techniques described in this paper in the initial conceptual phase of design informs engineers of the most efficient layout of material. Design decisions on the topology of the lateral system can therefore be streamlined with savings in material costs and minimization of impact on natural resources.

1.2. On existing frame optimization techniques

Currently, structural engineering optimization techniques can be classified into two distinct categories: discrete member optimization using beam or truss elements [6–10] and continuum methods [11–13].

Within the class of discrete member techniques for structural systems, Takezawa et al. [14] proposed a method for frame elements where the design variables consist of the cross-sectional properties, including principle direction of the second moment of inertia. Fredricson [15] used a joint penalty and material selection approach with flexible joints. Kaveh and Shahrouzi [16] employed the ideas of graph theory to determine the member connectivity between the supports and load paths for bracing systems. Wang [17] optimized frame structures using the maximum bending moment as the design criteria.

On the other hand, in Bendsoe and Sigmund [13] several examples are given for the continuum topology optimization problem where "beams" are added by creating a long row of solid elements across the design domain, as in the case of a two-dimensional bridge where the solid area represents the deck. Similarly, Allahdadian and Boroomand [2] proposed a technique using continuum elements to determine the optimal bracing system for dynamic response in designing or retrofitting structures. In that method, the floor levels were modeled as solid rigid elements.

Another technique, explored in the work of Neves et al. [3], tailors the topology optimization design framework for stability problems. In such formulation, the objective function is the critical buckling load, rather than minimum compliance. The paper by Neves et al. [3] considers the design of a portal frame and a five-story frame, similar to the examples presented in this work. However, this previous approach models the structural frames with solid quadrilateral (Q9) elements, instead of discrete (beam) elements, as presented in what follows. Furthermore, structural frame studies were presented with a specific natural frequency as the objective in the work of Diaz and Kikuchi [18].

While each of the aforementioned techniques in the literature is valuable in itself, better structural engineering tools may be developed by combining such ideas. Several attempts have been made at proposing an integrated structural optimization framework. For instance, Liang's technique [19,20] uses a performance index based on strain energy density for the optimization of multistory steel building frameworks. An existing frame is modeled of discrete steel elements with an underlying continuum mesh of quadrilaterals, which are removed based on the lowest performance indices. Mijar et al. [21] uses Reuss and Voigt mixing rules for effective stiffness with topology optimization to design bracing systems. Beam elements are used to model an unbraced system and continuum elements model the bracing layout. In Lagaros et al. [22], optimization has been taken a step further into the structural engineering industry by combining sizing, shape and topology optimization to design three-dimensional steel structures with web openings in compliance with modern design codes. Size optimization was used to determine the cross-sectional area of the beams and columns, while shape and topology optimization was implemented for the number and size of web openings. Here, we use a topology optimization approach with Solid Isotropic Material with Penalization (SIMP) where beam elements are included in the finite element analysis portion to achieve more meaningful bracing layouts. These layouts are derived analytically to verify the numerical results as well.

1.3. Paper scope and organization

This paper is organized as follows: in the next section, we discuss the main concepts of an energy-based method to efficiently size structural frames using the least amount of material. Following, energy methods, in conjunction with the Principle of Virtual Work (PVW), are used to mathematically derive the optimal geometry of a discrete braced structure in Section 3. Then, we outline the main concepts behind the combination of Q4 and beam elements, including several methods to attach the two types of elements. In Section 5, the topology optimization framework is introduced and extended to include simultaneous use of several element types in the context of structural framing systems. Some fundamental modeling aspects associated with the combination of beam and quadrilateral elements on a single module of a frame are investigated in Section 6 and compared to the results from Section 3. Finally,

numerical results are illustrated in Section 7 and conclusions are drawn on the application of the proposed methodology in the last section.

2. A sizing technique for frame optimization

In this section, energy methods and the PVW are explored to compliment the methodology for topology optimization of structural braced frames by introducing a sizing technique for the final beam, column and bracing members.

2.1. Applying energy methods to size braced frames

Baker [23] derived a method to calculate the optimal cross-sectional area for a statically determinate frame to limit the tip displacement of a building under wind load to a target deflection, Δ, by combining the PVW and the Lagrangian multiplier method. This methodology is based on the assumption that given a frame with axial forces due to a lateral load (e.g. wind load), F_i, length of members, L_i, and cross-sectional area, A_i, the target deflection can be achieved through strategic sizing of the cross-sectional areas. In this procedure, two load cases are analyzed: the real (wind) load case to calculate the strains and displacements (Fig. 3 (left)), and the virtual (unit) load case to calculate the stresses and forces (Fig. 3 (right)). Using the PVW, the work done by the virtual (unit) system for the displacement and deformation of the real (wind load) system can be written as follows:

$$\Delta \cdot 1 = \sum_i \int_0^{L_i} f \epsilon \, dx = \sum_i \int_0^{L_i} f \frac{F}{EA} \, dx = \sum_i \left(\frac{FfL}{EA}\right)_i \tag{1}$$

where $\epsilon = F/(EA)$ represents the strain in the real system, and f is the internal force of a member in the virtual (unit) system. Thus, the virtual work yields the following expression:

$$\Delta = \sum_i \left(\frac{FfL}{EA}\right)_i \tag{2}$$

Combining the PVW with the Lagrangian multiplier method, one obtains

$$\Delta = \sum_i \frac{F_i f_i L_i}{E_i A_i} + \lambda \left(\sum_j A_j L_j - V\right) \tag{3}$$

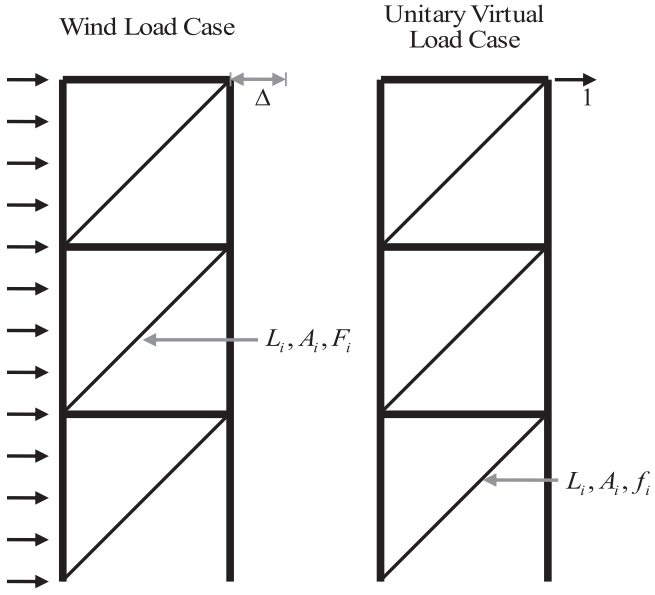

Fig. 3. Illustration of the PVW: real (wind) load case (left) and virtual (unit) load case (right).

where λ is the Lagrange multiplier, A_i is the unknown cross-sectional area of a member and $\left(\sum_j A_j L_j - V\right)$ is a constraint on the volume V of material. We note that additional constraints could be introduced using additional Lagrange multipliers.

By differentiating the above expression with respect to A_i and performing several numerical manipulations, the optimal cross-sectional area of a member for the target deflection, Δ_{req}, is determined from

$$(A_i)_{req} = \frac{1}{\Delta_{req} E} (F_i f_i)^{0.5} \left[\sum_j L_j (F_j f_j)^{0.5}\right] \tag{4}$$

The above expression provides optimal cross-sectional areas for a statically determinate braced frame. As shown in Baker [23], expressions similar to Eq. (4) can be derived for moments, shear and torque. Therefore, this sizing technique can be extended to moment frames provided that the moment of inertia, I, of the member is a linear function of the area, A, in the form $I = kA$, where k is a proportionality constant.

2.2. Overall design process

The optimization techniques described previously help streamline the design decisions at various stages of a project from the conceptual characterization of a braced frame layout to the final sizing of the members. Once the overall shape of the building is known, the optimal brace layout could be established assuming that frame columns are arranged at its outer perimeter at a regular spacing to ensure that the tributary areas for the columns are similar. At each floor level, a horizontal beam (spandrel) would span between two adjacent columns. Beams and columns would be modeled using beam elements while the space bounded by two columns and two beams would be meshed using quadrilateral elements. After the finite element mesh is completed the following steps can be applied in sequence in the design flow process (Fig. 4):

- size vertical line elements (columns) according to gravity load combinations (accounting for dead, superimposed dead and live loads);

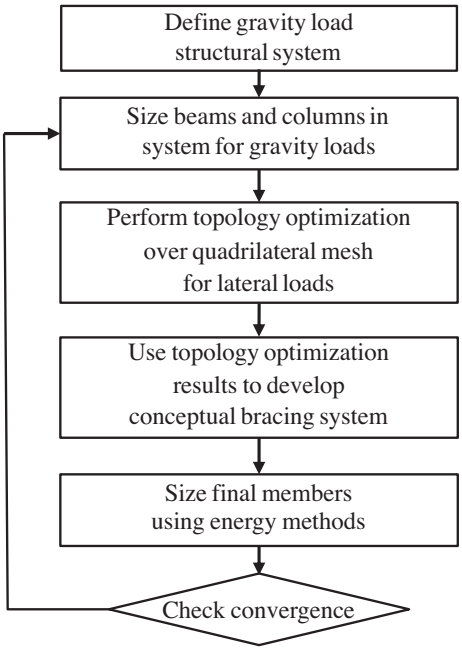

Fig. 4. Schematic for the overall optimization process of a braced frame.

- run topology optimization on the quadrilateral elements for lateral load combinations (accounting for wind and seismic loads);
- identify the optimal bracing layout based on the previous step and create a frame model consisting of beam elements;
- optimize the member sizes using the virtual work methodology

The above steps indicate a potential path from a conceptual design to the final sizing of a braced frame. However, each optimization step could be applied independently depending upon the specific need of the engineer. Notice that the distribution of loads shifts in the frame throughout the optimization process due to re-sizing of the members. Therefore, the process is iterative and should be repeated until convergence is achieved.

3. Optimal braced frames – analytical aspects

Important analytical aspects of optimal braced frames are explored in this section to establish a benchmark for comparison of the numerical results later presented in this paper.

3.1. Fully stressed design and optimal frames

The energy-based design method presented in Baker [23] and described in the previous section implies that any frame with optimal cross-sectional members subject to a point load at the top is under a state of constant stress (fully stressed design) as demonstrated in the following derivation. By taking the derivative of Eq. (3) with respect to the areas A_i and solving for the Lagrangian multiplier, we obtain:

$$\lambda = \frac{F_i f_i}{E A_i^2} \tag{5}$$

Considering a linear analysis, for the case of a point load at the top of the frame $f_i = k \cdot F_i$, where k is a proportionality constant, the following expression holds:

$$\lambda = \left(\frac{F_i}{A_i}\right)^2 \frac{k}{E} = const \tag{6}$$

In the above expression the Lagrangian multiplier is a constant, therefore the stress in the ith member, $\sigma_i = F_i/A_i$ is constant. The latter conclusion applies to any member i of the frame, thus the stress level is constant throughout the structure.

In the context of the statically determinate braced frame systems considered in this paper, the equivalence between a constant state of stress and minimum compliance is generalized from the single point load described above to multiple point loads P_i applied to the frame. Assuming that the displacements at each point of load application are u_i, the compliance can be expressed as:

$$W_{ext} = \sum_i P_i u_i = \sum_j \frac{F_j^2 L_j}{E A_j} = W_{int} \tag{7}$$

where W_{ext} and W_{int} are the work done by the external and internal forces respectively. By introducing the Lagrangian multiplier constraint on the areas of the members,

$$W_{ext} = \sum_j \frac{F_j^2 L_j}{E A_j} + \lambda \left(\sum_j A_j L_j - V \right) \tag{8}$$

In order to minimize the compliance of the system with various member sizes, the right-hand side of this equation is differentiated with respect to the areas A_i and solved for the Lagrangian multiplier λ to obtain the following:

$$\lambda = \left(\frac{F_i}{A_i}\right)^2 \frac{1}{E} = const \tag{9}$$

The above result is similar to Eq. (6) and confirms that, in the present context, minimum compliance leads to constant stresses. In general, for the compliance minimization problem, a state of *constant strain energy density* represents the *condition of optimality* [13]. Since the strain energy density is related to the Von Mises stress [24,25], the effective stresses in optimal structures are constant. Additionally, for the case of a single point load, minimum tip displacement coincides with minimum compliance. The constant stress condition is verified later for the continuum approach in Section 6.4.

3.2. Optimal single module bracing

Using the ideas from the previous section, we study the optimal geometry of the braced frame shown in Fig. 5, where the overall height of the frame is given as H, the total width as $2B$, and the height of the bracing intersection point as z. Notice that the problem in Fig. 5 (left) is simplified into the problem in Fig. 5 (right) by taking advantage of symmetry. Letting the height of the bracing point, z, be the design variable, we are looking for the optimal location that minimizes the deflection at the top of the structure using the PVW.

The frame shown in Fig. 5 is statically determinate, so by applying a unit load at the location of unknown deflection, Δ, the internal forces of the members can be solved for as follows:

$$f_1 = \frac{H - z}{B} \tag{10}$$

$$f_2 = \frac{\sqrt{B^2 + z^2}}{B} \tag{11}$$

and

$$f_3 = \frac{-\sqrt{B^2 + (H - z)^2}}{B} \tag{12}$$

Note that the forces in the frame induced by a wind load P applied at the same location as the unit load would simply be $F_i = P f_i$. Now, using Eq. (2) and assuming each member to have a constant stress, $\sigma = F_i/A_i$, the tip deflection is

$$\Delta = \frac{F_i}{E A_i} \sum_i f_i L_i = \frac{\sigma B}{E} \sum_i \frac{f_i L_i}{B} \tag{13}$$

The tip deflection of the frame is minimal when the following relationship holds:

$$\begin{aligned} \frac{\partial \Delta}{\partial z} &= \frac{\sigma B}{E} \frac{\partial}{\partial z} \left(\sum_i \frac{f_i L_i}{B} \right) = 0 \\ &= \frac{\sigma B}{E} \frac{\partial}{\partial z} \left(H \left(\frac{H - z}{B^2} \right) + \frac{B^2 + z^2}{B^2} + \frac{B^2 + (H - z)^2}{B^2} \right) = 0 \\ &= \frac{\sigma B}{E} \left(-\frac{H}{B} + \frac{2z}{B} - \frac{2(H - z)}{B} \right) = 0 \end{aligned} \tag{14}$$

Thus, the brace work point height for minimal deflection is

$$z = \frac{3}{4} H \tag{15}$$

This result is not surprising if we consider the problem in Fig. 6 (top). In this problem, a point load representing the wind (lateral) force acting on the frame is applied at the top left corner and symmetry is enforced. The topology optimization of the continuum mesh does not lead to a simple 45° bracing angle due to the interaction of shear and axial forces in a similar fashion to the one described in Section 4 of Stromberg et al. [1]. The 45° bracing angle would be the outcome of a pure shear problem as shown in Fig. 6 (bottom). However, the cantilever problem (used to model

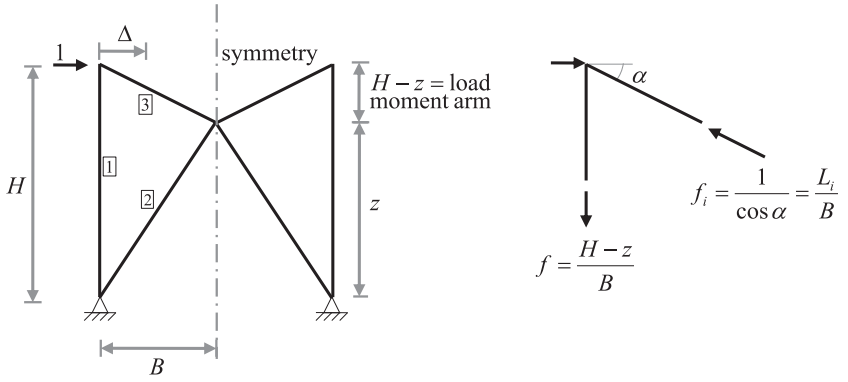

Fig. 5. Geometry and notation for the single module frame optimization problem with even number of diagonals.

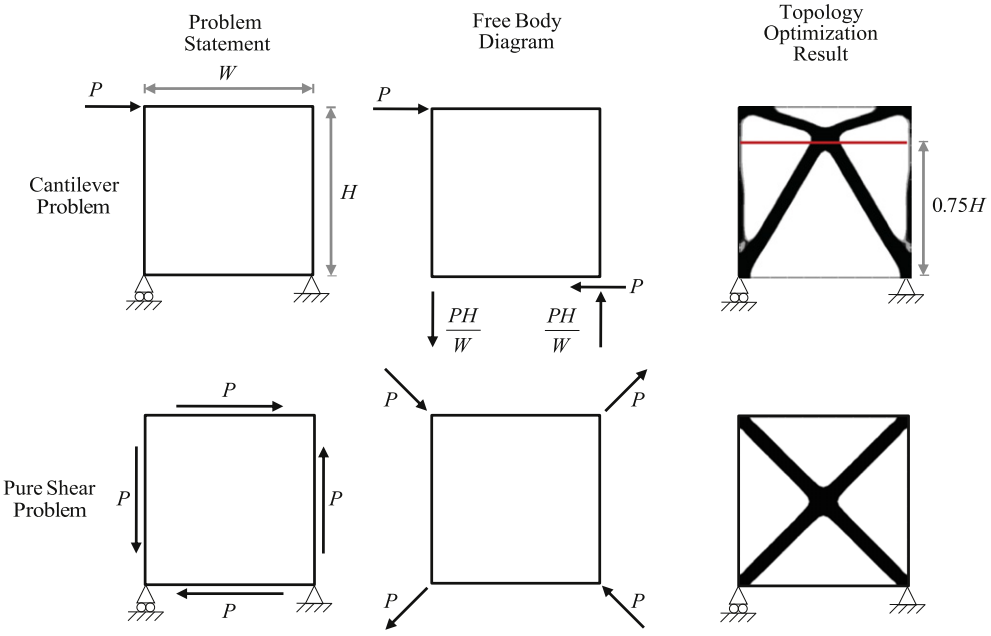

Fig. 6. Illustration of the differences between the case of a cantilever structure (top) and the pure shear problem (bottom).

a high-rise) is never pure shear because the overturning moment PH does not appear in a pure shear problem. Therefore, the topology optimization results in a "high-waisted" cross bracing. The actual location of the intersection point of the braces at 75% of the height H as shown in Eq. (15) is confirmed in Fig. 6 (top right).

This result has been further confirmed by running a simple Matlab code for discrete members as shown in Fig. 7. In the Matlab code, the intersection of the bracing was constrained to move along the centerline of the module due to symmetry, the height ratio, z/H, was varied from 0.5 to 1 (z being the distance of the brace work point from the base) and the corresponding tip deflection was calculated (see Fig. 7b). The optimal z/H ratio (i.e. the one that minimizes the deflection at the top of the frame) is shown to be $0.75H$ in Fig. 7b. The results here are contingent upon the assumption of constant stresses in the discrete members, which was demonstrated in the previous section.

3.3. Optimal multiple modules bracing for point load

The analysis conducted for a single module braced frame can be extended to a frame with multiple modules along the height and a single load applied at the top by observing the relationships between the geometry of the frames and the forces in its members as described by Figs. 5 and 8. The forces f_i in the diagonal members due to a unit point load at the top are (Fig. 5 (right) and Fig. 8 (right)):

$$f_i = \frac{L_i}{B} \tag{16}$$

while the forces in the columns are given by

$$f_i = \frac{(H - z_i)}{B} \tag{17}$$

where $(H - z_i)$ indicates the moment arm of the unit force in the module under consideration (see Figs. 5 (right) and 8 (right)). According to Eq. (16), the forces in the braces are dependent upon the length of the members and, in turn, are a function of the coordinates of the nodal elevations z_i. Combining Eq. (13) with Eqs. (16) and (17), the displacement at the top of the frame is

$$\begin{aligned} \Delta &= \frac{\sigma B}{E}\sum_i \frac{f_i L_i}{B} \\ &= \frac{\sigma B}{E}\left[\sum_i \left(\frac{L_i^2}{B^2}\right)_{braces} + \sum_j \left(\frac{(H - z_j)L_j}{B^2}\right)_{columns}\right] \end{aligned} \tag{18}$$

This expression is only a function of the nodal elevations z_i. Therefore, the frame of minimal tip deflection is obtained by taking the

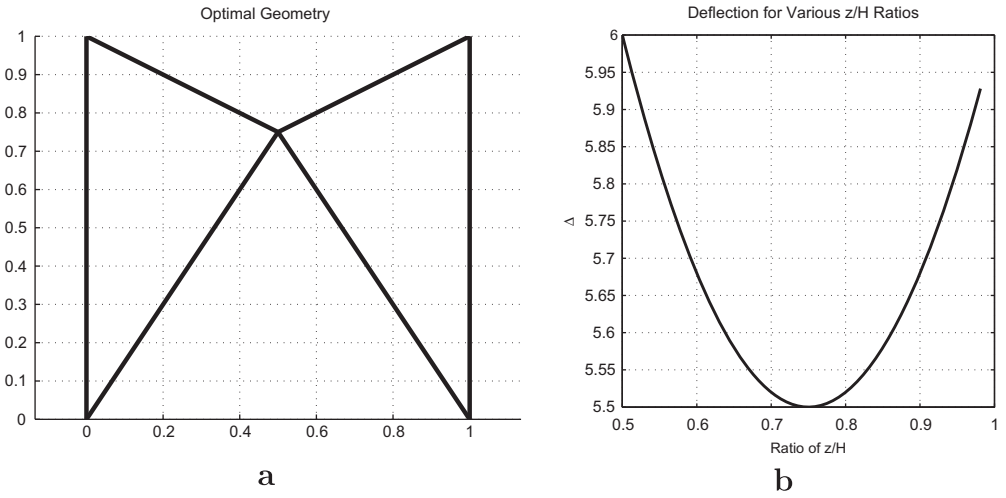

Fig. 7. Results for the optimization of the bracing angle for the cantilever problem: (a) optimal geometry for the truss and (b) plot of deflections versus brace height intersection ratio.

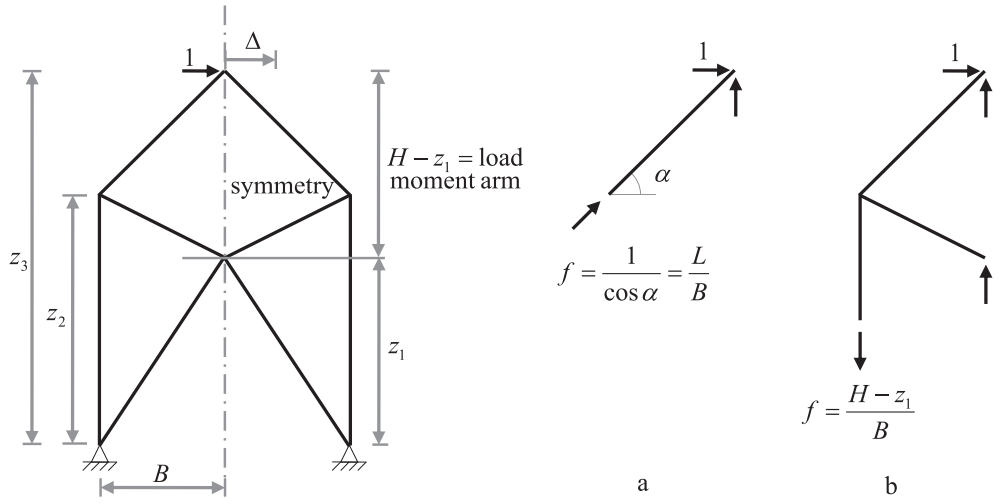

Fig. 8. Geometry and notation for the single module frame optimization problem with odd number of diagonals: (a) free body diagram for a diagonal member and (b) free body diagram for a column member.

partial derivatives of the above function with respect to the elevations z_i. For the frame in Fig. 8, as an example, the displacement is

$$\Delta = \frac{\sigma B}{E}\left[\sum_i \left(\frac{L_i^2}{B^2}\right)_{braces} + \sum_j \left(\frac{(H-z_j)L_j}{B^2}\right)_{columns}\right] = \frac{\sigma B}{E}\left[\frac{(H-z_2)^2}{B^2} + \frac{(z_2-z_1)^2}{B^2} + \frac{z_1^2}{B^2} + \frac{(H-z_1)z_2}{B^2}\right] \tag{19}$$

The frame with minimal top displacement is defined by the following equations:

$$\frac{\partial \Delta}{\partial z_1} = 0 \Rightarrow -3z_2 + 4z_1 = 0 \qquad \frac{\partial \Delta}{\partial z_2} = 0 \Rightarrow -H + 4z_2 - 3z_1 = 0 \tag{20}$$

Therefore,

$$z_1 = \frac{3}{4}z_2, \quad z_2 = \frac{4}{7}H \tag{21}$$

We observe that in the above equations the brace work point z_1 is still located at 75% of the height of the module z_2, similarly to the example described in Fig. 5. In addition, the top brace is parallel to the lower one, which hints to the presence of a pattern in the optimal solution.

3.4. Application to high-rise building patterns

The equations for the optimal work point elevations in a frame can be generalized to the case of the nth module of such a frame (see Fig. 9 for notation), where the top displacement of the frame can be expressed in terms of the dimensionless quantity, $E\Delta/(\sigma B)$, as follows:

$$\frac{E\Delta}{\sigma B} = \sum_{n=1}^{N} \frac{(z_{2n} - z_{2n-1})^2 + B^2}{B^2} + \frac{(z_{2n-1} - z_{2n-2})^2 + B^2}{B^2} + \frac{(H - z_{2n-1})^2}{B^2}(z_{2n} - z_{2n-2}) \tag{22}$$

Here N is the total number of modules and it is assumed that $z_{2n-2} < z_{2n-1} < z_{2n}$. By differentiating with respect to the nodal elevations z_{2n} (column work point) and z_{2n-1} (brace work point):

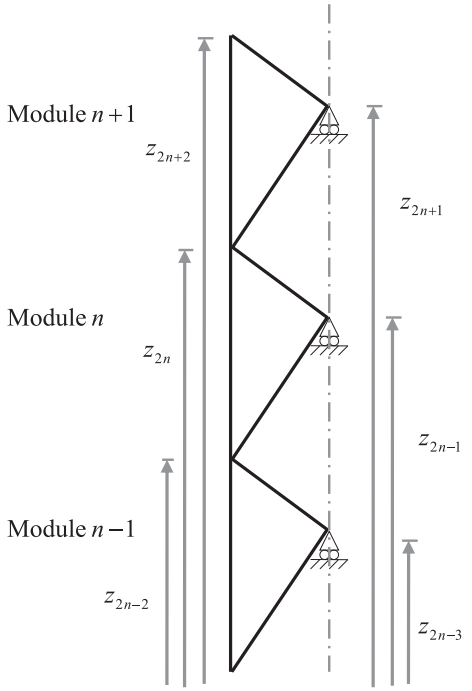

Fig. 9. Notation for the nth module of a frame (e.g. high-rise building).

$$\begin{aligned}\frac{\partial}{\partial z_{2n-1}}\left(\frac{E\Delta}{\sigma B}\right) = 0 \Rightarrow -3z_{2n} + 4z_{2n-1} - z_{2n-2} = 0\\ \frac{\partial}{\partial z_{2n}}\left(\frac{E\Delta}{\sigma B}\right) = 0 \Rightarrow -z_{2n+1} + 4z_{2n} - 3z_{2n-1} = 0\end{aligned} \tag{23}$$

These equations can be rewritten as follow:

$$\begin{aligned}z_{2n} &= \frac{z_{2n-1} + z_{2n+1}}{2} - \frac{z_{2n+1} - z_{2n-1}}{4}\\ z_{2n-1} &= \frac{z_{2n-2} + z_{2n}}{2} + \frac{z_{2n} - z_{2n-2}}{4}\end{aligned} \tag{24}$$

From the above expressions, two important geometric features of optimal braced frames are inferred:

1. The braced frame central work point z_{2n-1} is always located at 75% of the module height.
2. The module heights are all equal.

The last geometric property is easily verified in Fig. 10 where, after substitution, we obtain the relationship $z_2 = z_4/2$ for the two lowest modules. Similar relationships can be derived for the other modules.

3.5. Verification

To compare the validity of our results with those presented previously in the literature, we consider the optimum frameworks given in Hemp [26] based on the mathematics of optimal layouts first introduced in Michell [8]. In these previous works of literature, the authors aim to find the minimum volume required for a given structural framework and derive the conditions associated with such layouts. Using these conditions, Hemp derived the optimal geometry for the strip $0 \leqslant y \leqslant h$ consisting of cycloids. This problem can then be applied to the optimum design of 'shear bracing' of a long cantilever under a tip shear, F (given in 4.17 of Hemp [26]). The results of this study (see Fig. 11) are compared with

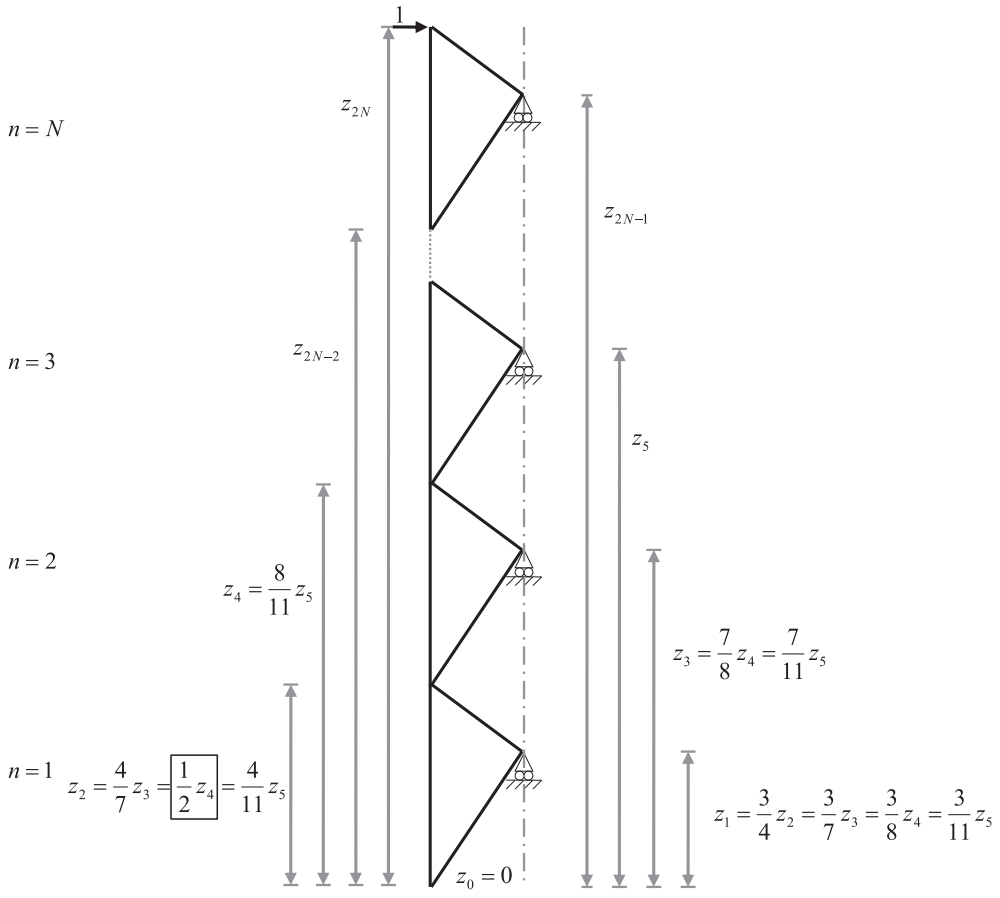

Fig. 10. Notation and geometric proportions for a frame with multiple modules and a single point load.

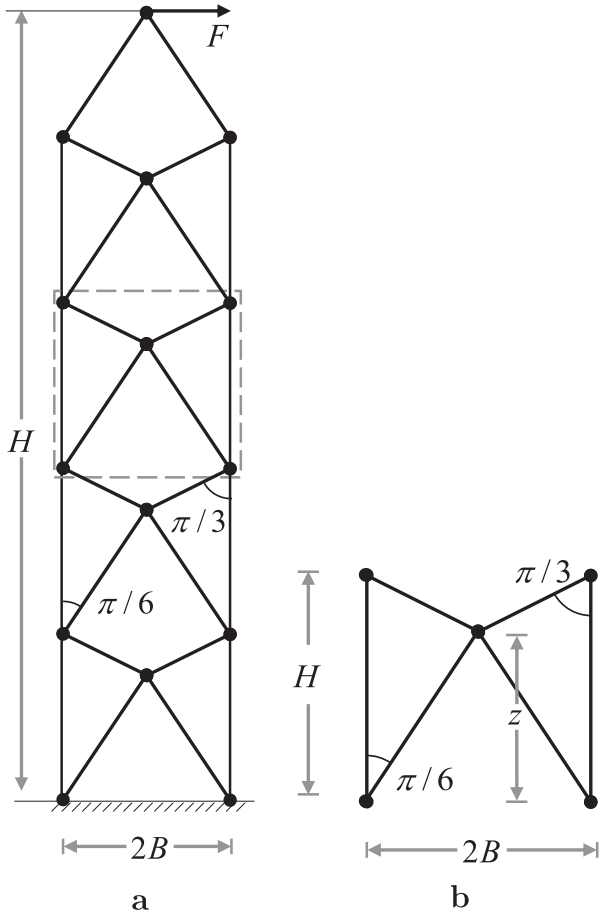

Fig. 11. Comparison of results with those of the literature: (a) Discrete truss showing the optimum shear bracing similar to that with a continuous array of orthogonal cycloids given in Hemp [26] (rotated by 90°) and (b) optimal geometry of a single module of the truss.

those presented in this work. Based on the angles of the optimal geometry derived by Hemp,

$$H = B\sqrt{3} + B\frac{\sqrt{3}}{3} = \frac{4\sqrt{3}}{3}B \tag{25}$$

we obtain

$$z = \frac{B\sqrt{3}}{\frac{4\sqrt{3}}{3}B} = \frac{3}{4} \tag{26}$$

thereby verifying the approach used by the authors.

3.6. Optimal number of modules for single point load

The results presented in the previous section identify geometric principles for optimal frames of minimum tip deflection and are independent of the aspect ratio H/B of the frame (see Eq. (24)). Therefore, one may wonder what is the optimal number of modules for a frame of given aspect ratio. This question is answered by minimizing the volume of the frame, which is written as follows:

$$V = \sum_i A_i L_i = \sum \frac{F_i}{\sigma} L_i = \frac{P}{\sigma}\sum_i f_i L_i = \frac{PB}{\sigma}\sum_i \frac{f_i L_i}{B} \tag{27}$$

where P is the magnitude of the unit load applied at the top of the frame, B is the width of each (symmetric) frame, and σ is the constant stress in each member. Noting the similarities between the above equation and Eq. (13), it follows:

$$V = \frac{PE}{\sigma^2}\Delta \tag{28}$$

Therefore, by minimizing the tip deflection Δ, the volume of the frame is also minimized. *In summary, the optimal frame for a point load is characterized by minimum tip deflection, minimum compliance, minimum volume and constant stress in the members.*

The problem for the optimal number of modules is formulated in terms of m, the optimal number of diagonals in the frame, as illustrated in Fig. 12. For example, with the geometry shown in Fig. 5 (or $m = 2$ in Fig. 12) the volume is

$$V = \frac{PB}{\sigma}\sum_i \frac{f_i L_i}{B} = \frac{PB}{\sigma}\left(\frac{H^2}{4B^2} + \frac{B^2 + \frac{9H^2}{16}}{B^2} + \frac{\frac{H^2}{16} + B^2}{B^2}\right) = \frac{PB}{\sigma}\left(2 + \frac{7}{8}\left(\frac{H}{B}\right)^2\right) \tag{29}$$

Similarly to the example above, the dimensionless frame volume $V\sigma/(PB)$ is derived for the other geometric configurations of Fig. 12 and the result is generalized for systems with m diagonal members in Table 1.

The dimensionless volume from Table 1 is computed and plotted in Fig. 13 for various aspect ratios H/B. The plot illustrates when the frame structure should transition, for example, from 1 to 3 diagonal members (see Fig. 13a), or 2 to 4 diagonal members (see Fig. 13b) and so on, by which volume curve is the lowest. The transitional aspect ratios are shown in the figure with a dashed vertical black line. The transition points can be derived analytically by equating the dimensionless volume of the frame with m diagonals to the one with $m + 2$ diagonals as follows:

$$\left(\frac{V\sigma}{PB}\right)_{m\text{diagonals}} = \left(\frac{V\sigma}{PB}\right)_{m+2\text{diagonals}} \tag{30}$$

Using the formulas derived in Table 1 for frames with an odd number of diagonals,

$$m + \left[\frac{m+2}{2m+1}\right]\left(\frac{H}{B}\right)^2 = m + 2 + \left[\frac{m+4}{2m+5}\right]\left(\frac{H}{B}\right)^2 \Rightarrow \frac{H}{B} = \sqrt{\frac{(2m+1)(2m+5)}{3}} \tag{31}$$

Similarly for a frame with an even number of diagonals,

$$\frac{H}{B} = \sqrt{\frac{2}{3}m(2m+4)} \tag{32}$$

In conclusion, the designer can first identify the optimal number of modules for a braced frame depending on the H/B ratio, then later identify the optimal bracing layout according to the geometric relationships described by Eq. (24).

Using this methodology, a conceptual design for a competition entry featuring optimal bracing work point locations was proposed by Skidmore, Owings & Merrill, LLP as shown in Fig. 14.

3.7. Optimal multiple modules bracing for multiple loads

The results for a frame with a single point load applied at the top are here generalized to the case of multiple point loads. Within this context, the optimality criteria followed is compliance minimization, which leads to a fully stressed design as described previously. The compliance (or external work of the applied forces W_{ext}) is written in the following dimensionless form:

$$\frac{EW_{ext}}{\sigma BF} = \sum_{n=1}^{N}\left[(N-n+1)\frac{(z_{2n}-z_{2n-1})^2 + B^2}{B^2} + (N-n+1)\frac{(z_{2n-1}-z_{2n-2})^2 + B^2}{B^2} + \left(\sum_{j=n}^{N}\frac{z_{2j}-z_{2n-1}}{B^2}\right)(z_{2n}-z_{2n-2})\right] \tag{33}$$

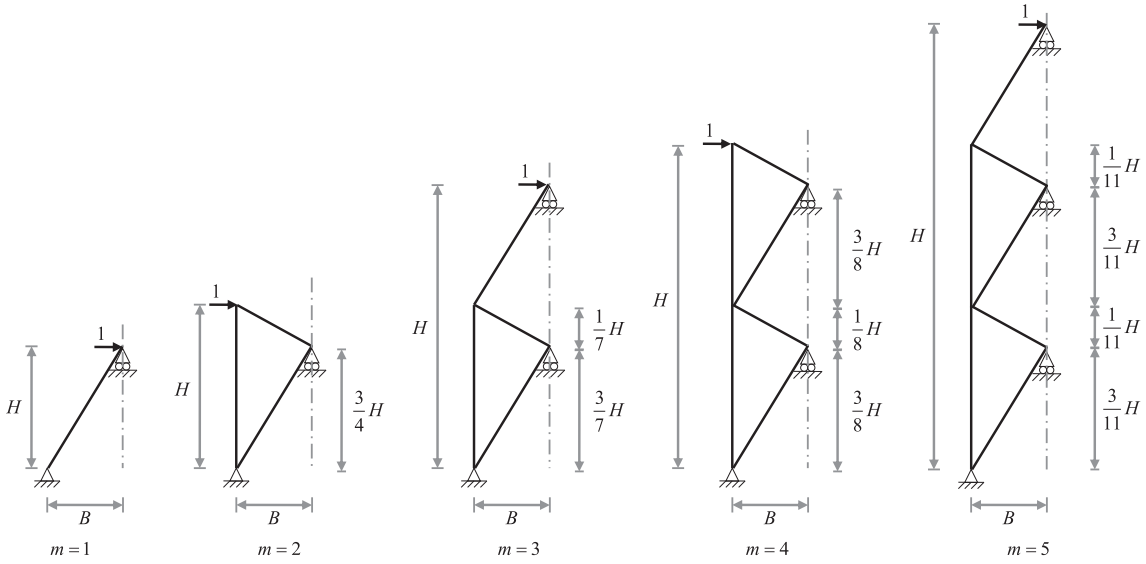

Fig. 12. Geometry and notation for optimal braced frames with m diagonal members.

Table 1
Frame volumes for various numbers of diagonals.

Number of diagonals, m	Dimensionless frame volume, $V\sigma/(PB)$
1	$1+\left(\frac{H}{B}\right)^2$
2	$2+\frac{7}{8}\left(\frac{H}{B}\right)^2$
3	$3+\frac{5}{7}\left(\frac{H}{B}\right)^2$
4	$4+\frac{11}{16}\left(\frac{H}{B}\right)^2$
5	$5+\frac{7}{11}\left(\frac{H}{B}\right)^2$
m (odd)	$m+\left[\frac{m+2}{2m+1}\right]\left(\frac{H}{B}\right)^2$
m (even)	$m+\left[\frac{1}{2}+\frac{3}{4m}\right]\left(\frac{H}{B}\right)^2$

The above equation is very similar to Eq. (22) derived for the case of a single point load. The minimum compliance is obtained by taking partial derivatives of this equation, as given for the case of the bracing work point location z_{2n-1} below:

$$\frac{\partial}{\partial z_{2n-1}}\left(\frac{EW_{ext}}{\sigma BF}\right)=0 \Rightarrow \frac{N-n+1}{B^2}(-3z_{2n}+4z_{2n-1}-z_{2n-2})=0 \tag{34}$$

This equation yields the same results presented in Eq. (23). Therefore, it is confirmed that even in the case of multiple point loads applied to the frame, the optimal bracing work point is located at 75% of the height of the module. Furthermore, the optimal height of a module can be derived by taking the partial derivative of Eq. (33) with respect to the column work point elevation z_{2n}. The frame modules are considered to be of constant height in what follows.

4. Combining Q4 and beam elements

In this section, the integration of beam and Q4 elements for two-dimensional problems is discussed with emphasis on the node-to-node connections or, more specifically, on the interaction among the coincident degrees of freedom.

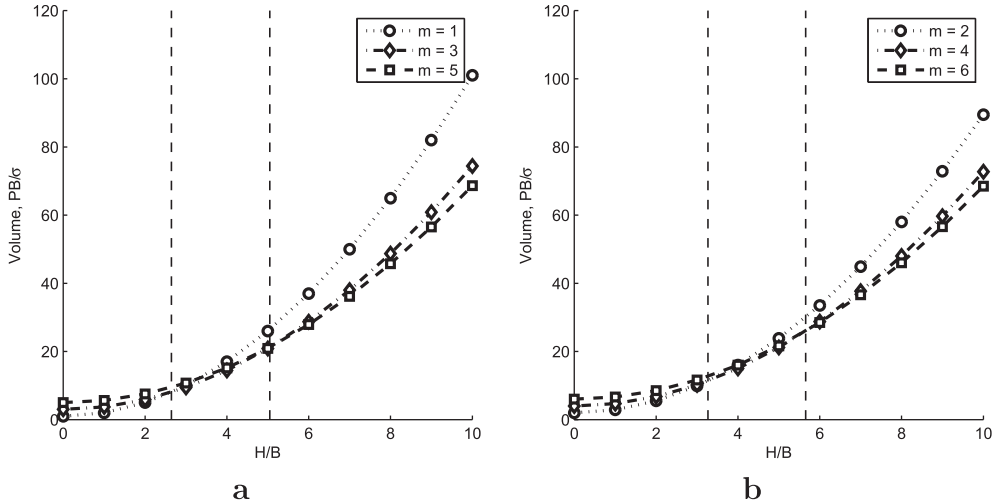

Fig. 13. Plot of dimensionless volume versus height to width ratio, H/B: (a) odd number of diagonals and (b) even number of diagonals.

Fig. 14. Rendering of a competition entry showing an optimal bracing system (image courtesy of Skidmore, Owings & Merrill, LLP).

4.1. Element combination alternatives

In the proposed technique, the element types used are the standard two-node beam elements with six degrees of freedom (two translations and one rotation at each node) and the four-node bilinear quadrilateral elements with eight degrees of freedom (two translations per node). In order to effectively connect the finite elements, the interaction between the rotational and translational degrees of freedom must be taken into account. This interaction can be carried out using the three methods outlined in Fig. 15:

- the beam element is attached only at the extreme ends of the quadrilateral mesh so interior nodes of the quadrilateral mesh along the beam move independently of the interior nodes of the beam element (Fig. 15a),
- the beam is discretized into many smaller beam elements which are attached at every node of the quadrilateral mesh along the beam line, forcing the quadrilateral nodes to translate together with the beam elements (Fig. 15b),
- the beam elements share all the degrees of freedom with the *enriched* quadrilaterals along the beam line, meaning each node of both quadrilaterals and beams must translate and rotate concurrently as opposed to the previous methodologies where the quadrilaterals were limited to pure translations (Fig. 15c).

Details of these implementations are discussed next, and a comparison of results based on these techniques is given later, in Section 6.2.

4.2. Beam and quadrilateral elements connected at extreme ends only

The first method for combining continuum and discrete finite elements consists of simply connecting the beam ends to the extreme corners of the quadrilateral mesh. As displayed in Fig. 15a, the beam elements share two translational degrees of freedom at each end (highlighted in red[1]) with the quadrilaterals. Thus, the end rotation of the beam has no influence on the quadrilateral finite elements because the rotational degree of freedom is decoupled. Additionally, all the interior nodes along the length of the beam are free to move independently of the quadrilateral node translations (see Fig. 16). Here, the effect of the beam elements is only global on the mesh, that is, the beams provide translational and rotational stiffness at the column node locations (Fig. 16).

4.3. Beam and quadrilateral elements attached continuously along beam line

In the second method for connecting the discrete and continuum elements (as shown in Fig. 15b), the horizontal beam is discretized into beam elements with nodes that coincide with the nodes of the quadrilateral mesh. Consequently, the translational degrees of freedom of both beam and quadrilateral elements are shared throughout the beam's length (shown in red). Thus, the quadrilateral elements are constrained to move jointly with the beam elements when the frame deforms. This behavior is illustrated in the sketch shown in Fig. 17.

Note that the connection between beams and columns in a structural steel frame can be designed for various degrees of moment transfer (i.e. shear connections, flexible moment connections, moment connections (see Fig. 18), which correspond to various rotational stiffness levels for the connection. The influence of the connection stiffness on the topology optimization results is studied later through numerical examples.

4.4. Beam and enriched (drilling) quadrilateral elements attached continuously along beam line

Bilinear quadrilateral (Q4) elements behave poorly in in-plane bending; however, inclusion of additional drilling degrees of freedom allows the enriched elements (Q4D4), illustrated by Fig. 19, to perform better than the four-node quadrilateral elements (Q4) while using less degrees of freedom than the eight-node quadrilateral (Q8) [27]. Here, the two translations at the middle nodes in the Q8 are converted to one rotation at each corner in the Q4D4 element (see Fig. 19). The equations for the drilling degrees of freedom can be derived from the basic Q8 formulation [27] as follows:

$$\begin{pmatrix} u_m \\ v_m \end{pmatrix} = \frac{1}{2}\begin{pmatrix} u_i \\ v_i \end{pmatrix} + \frac{1}{2}\begin{pmatrix} u_j \\ v_j \end{pmatrix} + \frac{\theta_j - \theta_i}{8}\begin{pmatrix} y_j - y_i \\ x_i - x_j \end{pmatrix} \tag{35}$$

where u_i and v_i are the horizontal and vertical translations at node i, θ_i is the pseudo-rotation at node i, m represents a mid-span node, and i and j are the corner nodes of the element.

Though the additional drilling degrees of freedom allow the quadrilateral elements to rotate or bend with the beam elements along the beam line, as observed in Fig. 20, no significant influence has been observed on the optimization (compliance) results. This behavior can be explained by observing that the additional rotations provided by the drilling degrees of freedom capture only a local bending effect. Therefore, standard Q4 elements are sufficiently accurate to represent the structural behavior of the examples shown in this paper since the translational behavior is dominant. Note also that the Q4D4 implementation is computationally more expensive than that using ordinary Q4 elements.

5. Topology optimization formulation

The integration of beam and quadrilateral elements described in the previous section can be incorporated into the classical topology optimization formulation by introducing a few modifications as described below.

[1] For interpretation of color in Figs. 2, 6, 14, 15, 21, 24, and 27–29, the reader is referred to the web version of this article.

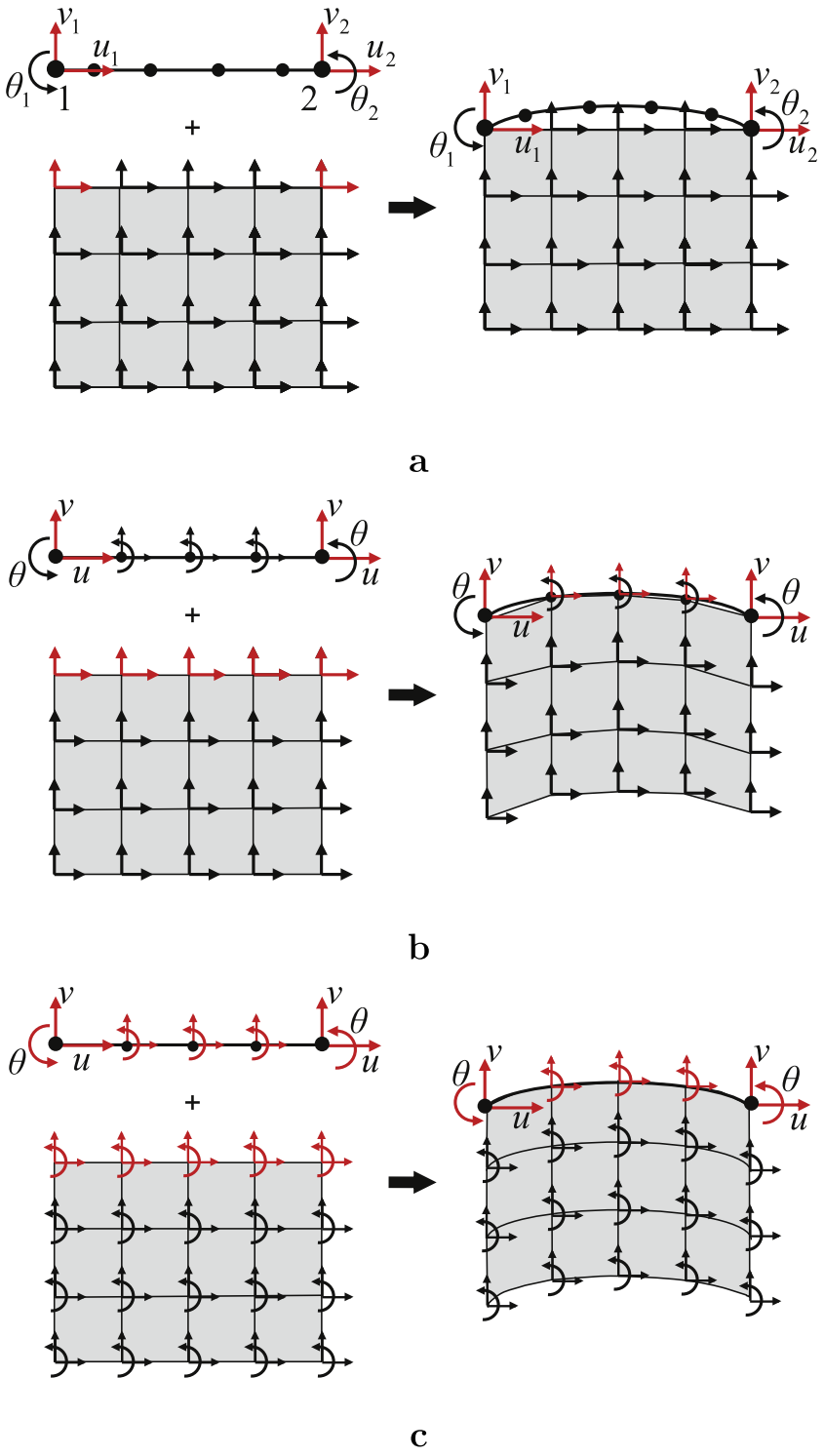

Fig. 15. Connection types for beam and quadrilateral finite elements: (a) attached at global beam ends, (b) attached at all concurrent mesh nodes, and (c) attached at all concurrent mesh nodes with enriched (drilling) Q4 elements.

5.1. Problem statement

Despite several objectives (tip displacement, frequency, buckling, compliance, etc.) in topology optimization, in this work we choose to maximize the overall stiffness of a building; thereby, minimum compliance is used as the objective function of the optimization. The design domain of the buildings considered in this paper is the outer skin or shell. The optimal layout in terms of minimum compliance can be stated in terms of the density, ρ, and the displacements, $\mathbf{u}$, as follows:

$$\begin{aligned} &\min_{\rho,\mathbf{u}} \quad c(\rho,\mathbf{u}) \\ &\text{s.t.} \quad \mathbf{K}(\rho)\mathbf{u} = \mathbf{f} \\ &\int_{\Omega} \rho \, \mathrm{d}V \leqslant V_s \\ &\rho(\mathbf{x}) \in [0,1] \quad \forall \mathbf{x} \in \Omega \end{aligned} \tag{36}$$

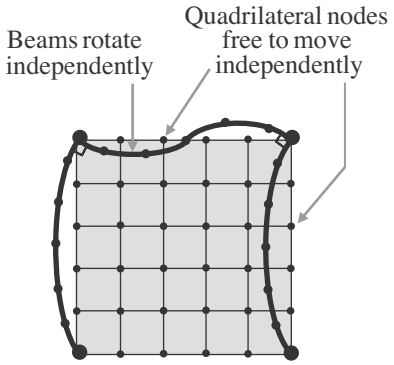

Fig. 16. Simple moment frame demonstrating a sample displacement field where beam elements rotate independently of the nodal translations of the quadrilateral elements along the beam line.

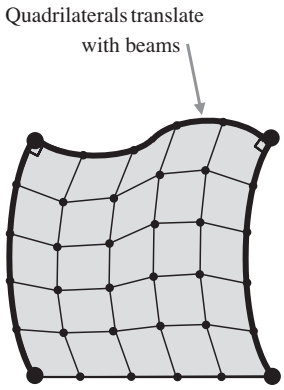

Fig. 17. Example of a displacement field with beam and quadrilateral elements attached continuously along beam line.

In the above equations c represents the overall compliance of the structure while $\mathbf{K}(\rho)$ represents the global stiffness matrix which depends on the material densities, $\mathbf{u}$ and $\mathbf{f}$ are the vectors of nodal displacements and forces, respectively, V_s is the volume fraction constraint which represents the maximum volume of material permitted for the design of the structure, and ρ is the material density for each design variable where $\rho = 0$ signifies a void and $\rho = 1$ represents solid material.

The ill-posedness of the topology optimization problem, or lack of a solution in the continuum setting [28–30], can be overcome through relaxation. A continuous variation of density in the range $[\rho_{min}, 1]$ is applied in relaxation rather than restricting each density to an integer value of 0 or 1 thereby guaranteeing the existence of a solution. A small parameter greater than zero, ρ_{min}, is specified to avoid singularities of the global stiffness matrix, $\mathbf{K}(\rho)$.

The topology optimization problem is solved by means of the SIMP model [31,32,12,33], however, other material models may be used, such as the Rational Approximation of Material Properties (RAMP) [34,13]. In the SIMP formulation, a power-law relation between the stiffness and element density is introduced in the form:

$$\mathbf{E}(\mathbf{x}) = \rho(\mathbf{x})^p E_0 \tag{37}$$

where E_0 describes Young's modulus of the solid material and p is a penalization parameter with $p \geqslant 1$. This formulation prescribes that the material properties continuously depend on the material density at each point. The penalization parameter, p, forces the material density towards 0 or 1 (void or solid respectively) as opposed to forming regions of intermediate densities (gray zones) where ρ assumes a value somewhere between 0 and 1. The optimization procedure presented in this work uses continuation, where the penalization parameter, p, is increased over the range of 1 to 4, in increments of 0.5 until convergence at each value is achieved.

5.2. Projection methodology with continuum and discrete elements

To avoid the common problem of checkerboarding over the quadrilateral mesh, a projection technique, similar to that of Guest et al. [35], was implemented. In addition to eliminating the checkerboarding patterns, projection is used as a means to specify the minimum member size (characteristic length) in a structure. The projection method in this work was performed only over the quadrilateral mesh since the discrete members already have a given cross-sectional area. Moreover, the presence of the beam or column elements should have no influence over the topology optimization of the bracing members since they are already members as

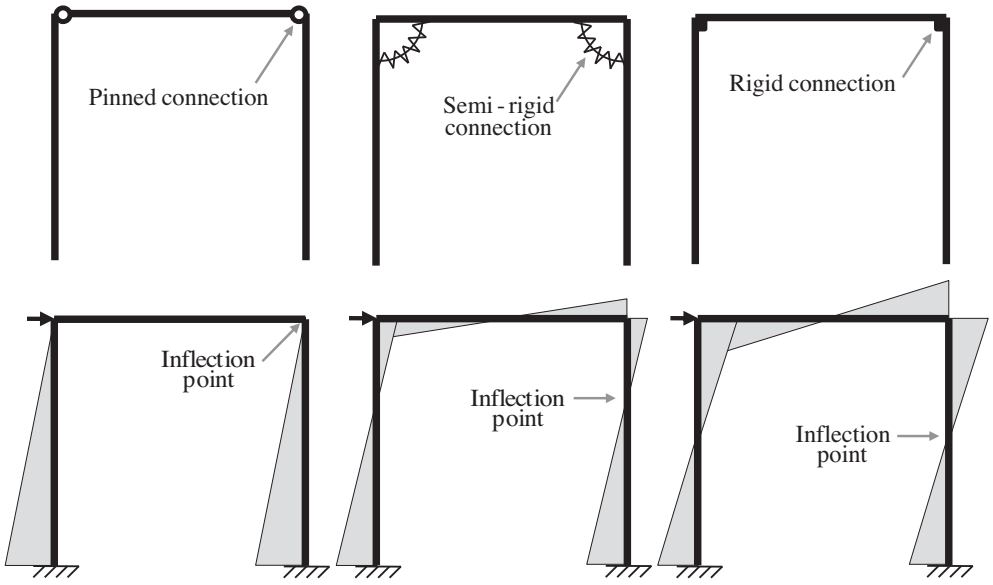

Fig. 18. Analytical representation of the beam to column connections of various stiffness and corresponding moment diagrams. From left to right: shear connection, flexible moment connection, moment connection.

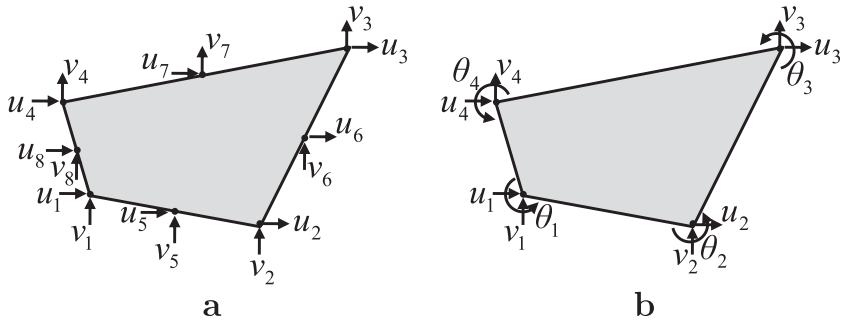

Fig. 19. Addition of drilling degrees of freedom using the mid-side displacements: (a) 8-node quadrilateral element (Q8) and (b) 4-node quadrilateral element with additional rotations (Q4D4).

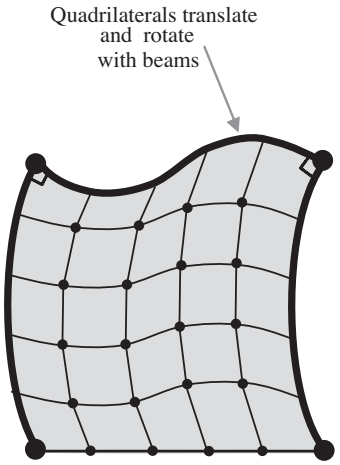

Fig. 20. Example of a displacement field with enriched (drilling) quadrilateral elements (Q4D4).

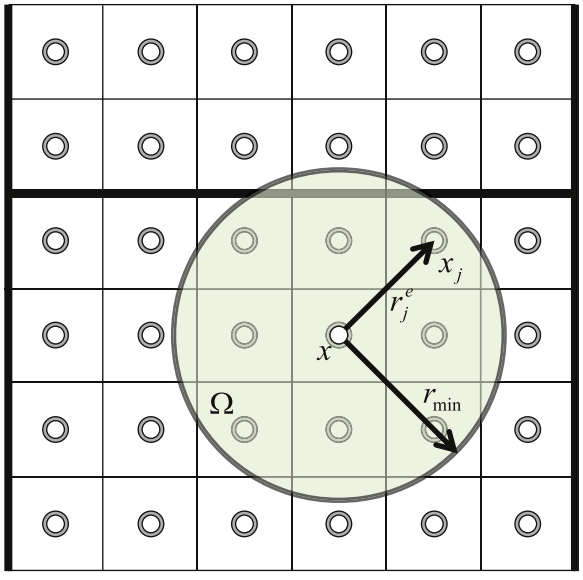

Fig. 21. Minimum length scale for projection technique over quadrilateral elements; beam and column elements that lie within the radius have no effect on continuum topology optimization.

illustrated in Fig. 21. The optimality criteria [36] is used for the optimization process.

6. Discussion on finite element modeling assumptions

In this section, the behavior of a single module of a high-rise building is studied to understand some fundamental modeling aspects that arise from combining discrete and continuum elements. Furthermore, we discuss how various modeling assumptions affect the final topology of the lateral bracing system for a high-rise building. For the following problems, we assume an equal height and width of 10 ft with W10×30 steel columns (as specified). For the topology optimization problem, the volume fraction is 30% with a projection radius of 6 in.

6.1. Influence of point load application in the context of symmetry

The application of the symmetry constraint is studied for the load case in Fig. 22. If only one load is applied at the top left corner of the mesh and symmetry is enforced, the top member is crucial to transfer the load to the column on the far side. This conclusion holds when the mesh has quadrilateral elements only (Fig. 23a), as well as when beam elements are introduced for the columns (Fig. 22a). With the application of two loads (one at each top corner in the same direction) there is no need for the horizontal member to transfer the load to the far sided column. Therefore, such members disappear from the topology optimization layout (Fig. 22b and 23b).

Moreover, in Fig. 23, column elements were absent from the mesh and the resulting K-brace in Fig. 23a shows almost disappearing columns. This is consistent with the static equilibrium at the node illustrated in Fig. 24 (left). Similarly, the result in Fig. 23b is consistent with the free body diagram in Fig. 24 (right). Moreover, in the presence of vertical loads the column members would always be required to transfer such loads from the building structure to its foundation.

In the numerical examples in this paper, the symmetry condition was applied using the schematic illustrated in Fig. 22b since the lateral load considered is a wind load which has a windward and a leeward component.

6.2. Effect of beam to quadrilateral element connection on the optimal topology

The effect of the various beam to quadrilateral element connections as described in Section 4 are investigated in Fig. 25. Fig. 25a corresponds to the situation described in Fig. 16 where only the extreme beam ends (black nodes) are attached to the Q4 mesh. Since the nodes are unattached along the beam line and the column line, and the moment is transferred from the beam to the column, the bracing developed stiffens the moment frame.

Fig. 25b corresponds to the situation described in Fig. 17 where the beam and column displacements are tied to those of the

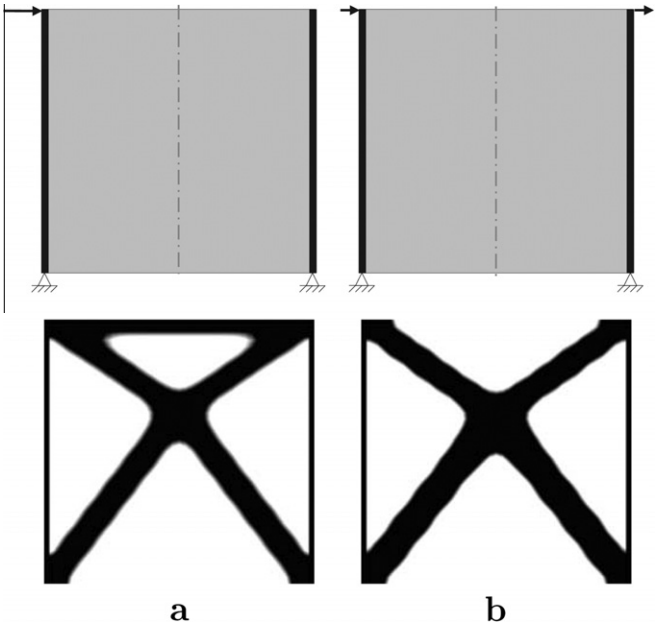

Fig. 22. Influence of symmetry constraint on mesh with 6400 quadrilateral (Q4) elements and 2 beam (W10×30) elements: (a) single point load with symmetry applied to the optimization and (b) anti-symmetric point loads with symmetric result.

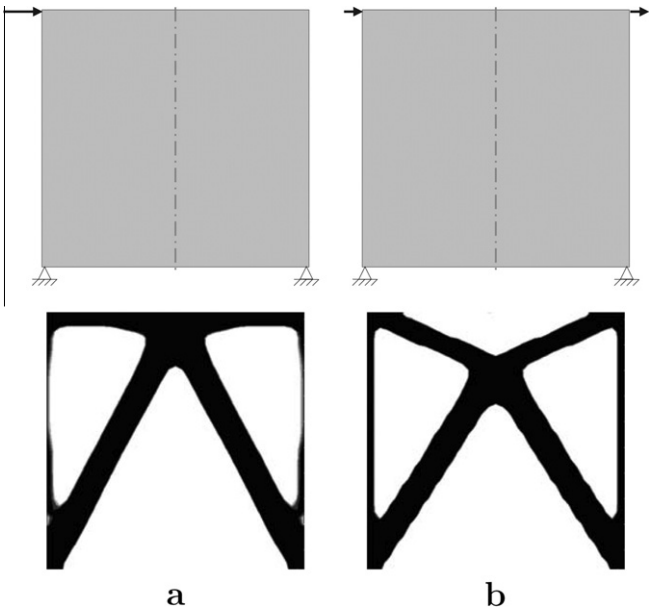

Fig. 23. Influence of symmetry constraint on mesh with 6400 quadrilateral (Q4) elements (no columns): (a) single point load with symmetry applied to the optimization and (b) anti-symmetric point loads with symmetric result.

quadrilaterals (at the black nodes). Thus, the optimal bracing engages the frame at intermediate working points along the lengths of the beams and columns.

Fig. 25c represents a situation similar to Fig. 25b, the only difference being the moment release (drawn as a hollow circle) at the extreme ends of the beam. As a consequence, the moment is no longer transfered between the beam and column and a stiffening pattern for the corners develops. In order to evaluate the solution with the best structural performance, we consider the final compliance of the three frames in Fig. 25: (a) 0.3287, (b) 0.3397,

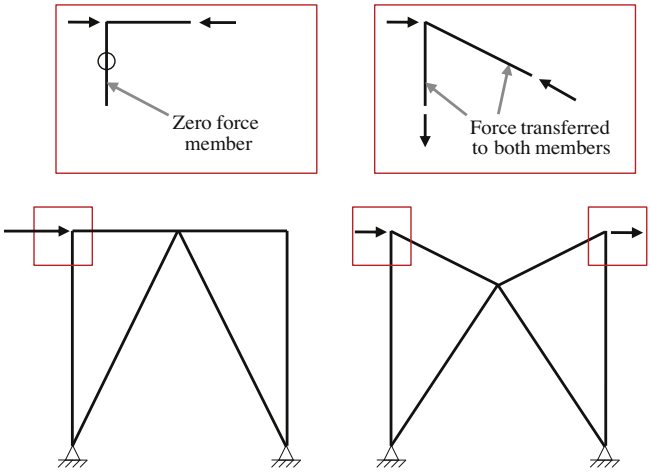

Fig. 24. Effect of asymmetric versus anti-symmetric load application on column elements: (left) K-brace develops zero-force "columns"; (right) presence of forces in column members of high-waisted brace.

and (c) 0.3525. Since the volume of material is the same for all the frames, from an engineering standpoint, if no other constraints are present, the best performing frame would be the braced frame in Fig. 25a.

6.3. Influence of the column stiffness on the bracing layout

The effect of varying the column area while keeping the continuum mesh unchanged subject to anti-symmetric point loads at the top corners (see Fig. 22b) is demonstrated in Fig. 26. The dimensions of this module are taken to be 48 m by 41.5 m. An anti-symmetric point loading of $P = 2$ MN is applied to the top corners. The area, A_0, of the column elements in Fig. 26a were sized to achieve a uniform stress in accordance with the conditions of optimality for compliance described in the previous sections. Thus, we select an area of $A_0 = 0.0021$ sq m for the column elements, a thickness of $t = 0.002$ m for the Q4 elements and $E = 200,000$ MPa (steel). For the topology optimization, a volume fraction of 20% is used with a projection radius of $r_{min} = 3$ m.

As the area, A, is increased from the optimal area, A_0, the intersection of the cross-brace (working point) moves vertically downward towards the 45° bracing solution. Fig. 26 shows the importance of proper sizing of the columns to obtain the theoretical optimal solution. Correspondingly, the proportions between the radius of gyration of the columns and the overall width of the domain would also be of influence to the bracing point, i.e. the higher this ratio, the lower the bracing point. However, in practice the columns would first be sized for gravity loads and later designed for lateral loads. Therefore, the column area may be higher than the optimal area, and furthermore demonstrate a lower work point than the 75% solution.

6.4. Verification of the constant stress condition

As described earlier in Section 3.1, the constant stress condition is verified in the continuum approach for the previous structure in Fig. 27 (left) which was derived using a Q4 element mesh. As shown in Fig. 27 (right), the Von-Mises stresses are nearly constant within each optimized member.

7. Optimal braced frames – numerical results

Numerical applications of the methodology developed in this paper are presented in this section for the case of a

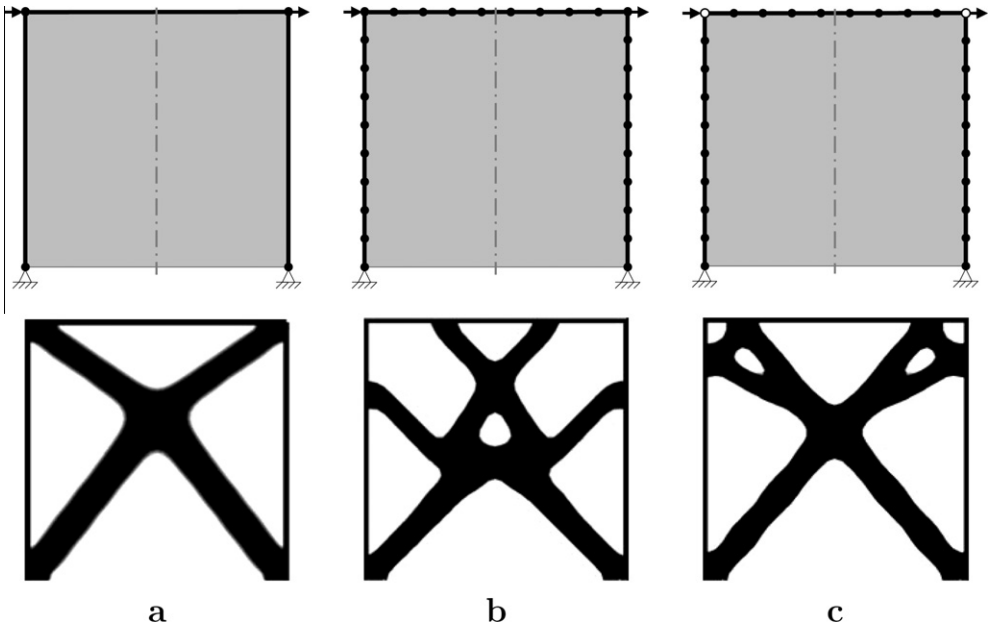

Fig. 25. Effect of different beam to quadrilateral connection types as presented in Section 4: (a) attached at global beam ends with mesh of 6400 Q4 and 3 W10×30 beam elements, (b) attached at all concurrent mesh nodes with mesh of 6400 Q4 and 120 W10×30 beam elements, and (c) attached at all concurrent mesh nodes with moment release for mesh of 6400 Q4 and 240W10×30 beam elements. Nodes shown in black indicate beam to quadrilateral connection.

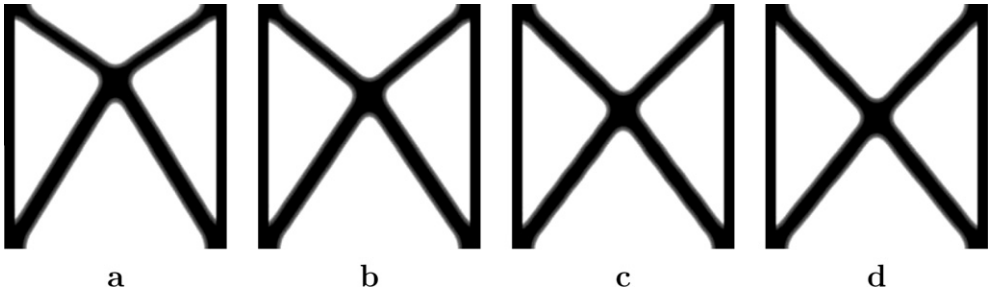

Fig. 26. Effect of varying the stiffness of the column elements on the optimal bracing layout with mesh of 6400 Q4 elements and two beam elements: (a) $A = A_0$, (b) $A = 2A_0$, (c) $A = 5A_0$, and (d) $A = 10A_0$. Intersection of bracing approaches 50% of height as column area is increased from the optimal solution.

two-dimensional high-rise building frame. Such examples portray several features of optimal frames that were described in the previous sections.

First, the problem given in Hemp [26] is solved using the combined approach in Fig. 28. In this problem, the overall dimensions of the structure are given as $H = 276$ m by $2B = 41.5$ m. The loading considered is a lateral load of $P = 1000$ kN applied at the top center with a symmetry constraint across the y-axis. This structure is assumed to be made of steel, with $E = 200$ GPa. Using the virtual work methodology to satisfy the drift limit requirements as described in Section 2 and assuming constant stress as described in Section 3.1 applied to the analytical solution for 11 diagonals based on the truss geometry of Fig. 12, the total volume of the structure was computed to be 48 m^3, where the columns account for 35 m^3 of this value and the bracing accounts for 13 m^3. The column sizes established using the analytical solution were carried over to the numerical solution.

Using the discrete/continuum element combination, the topology optimization problem is run with continuation on the penalization from $p = 1$ to 4 in steps of 0.5 with a projection radius of $r_{min} = 3$. As seen in Fig. 28b the thick areas of material are no longer concentrated at the edges of the domain. Furthermore, the braces are now complete and clearly defined and the final geometry produces the same angles as shown in the benchmark example of Fig. 11. Moreover, the resulting diagonal "members" are equal in size and the stresses are nearly constant throughout the height. As was stated previously, for intermediate densities the Von Mises stresses will be constant since the strain energy is constant. The regions where the stresses are higher (or lower) are when the densities are at the endpoints of the [0,1] range (i.e. a density of 1 gives a higher stress and a density of 0 gives a lower stress than the constant). This example verifies the numerical methodology to identify the optimal bracing layout.

Next, in reference to the results shown in the introduction, we study the addition of discrete truss elements (columns) from Fig. 1c in more detail here. In this problem, the overall dimensions of the structure are given as $H = 288$ m by $2B = 41.5$ m. The loading considered is a lateral load of $P = 2000$ kN applied at each module with a symmetry constraint across the y-axis. This structure is assumed to be made of steel, with $E = 200$ GPa. Using the virtual work methodology to satisfy the drift limit requirements as described in Section 2 and assuming constant stress as described in Section 3.1 applied to the analytical solution for six modules based on the truss geometry of Fig. 12, the total volume of the structure was computed to be 240 m^3, where the columns account for 35% of this value and the bracing accounts for 20%. The column

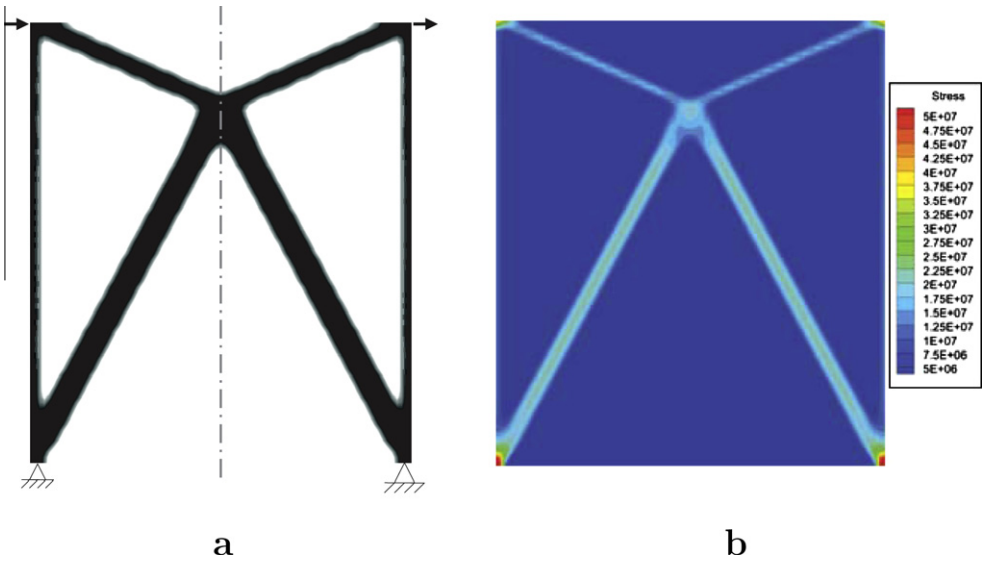

Fig. 27. Topology optimization of a frame using 6400 quadrilateral elements (left) and corresponding plot of Von Mises stresses (right).

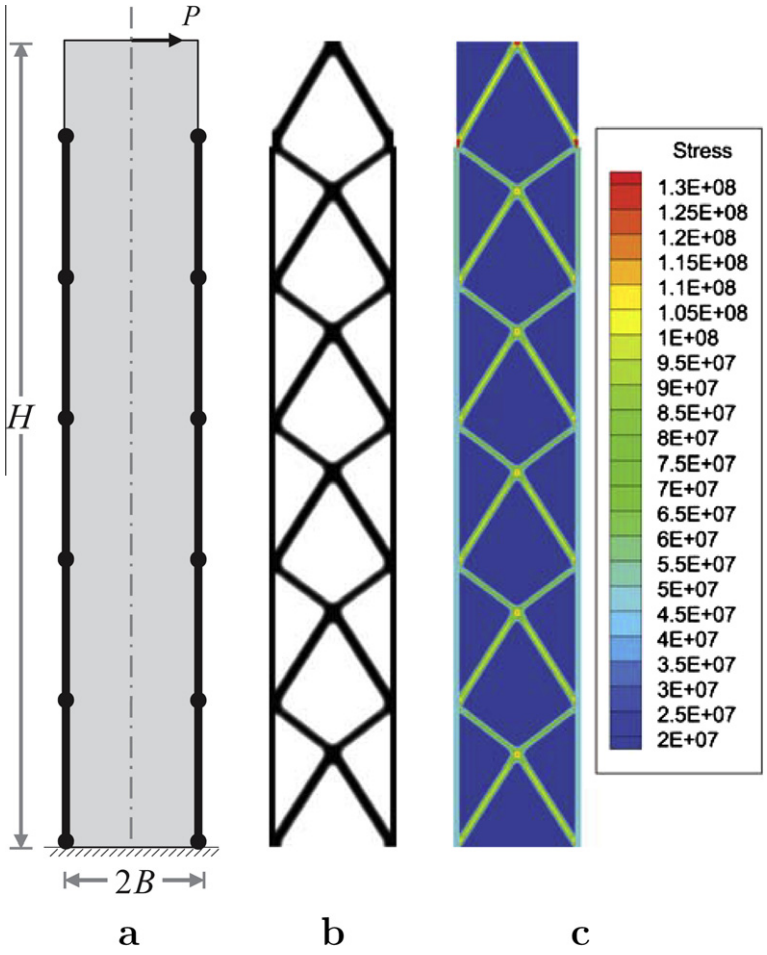

Fig. 28. Topology optimization for braced frame given in Hemp [26]: (a) problem statement, (b) topology optimization result, and (c) stress distribution.

sizes established using the analytical solution were carried over to the numerical solution. Similarly, the volume fraction for the topology optimization problem was then taken to be 20% of solid material.

The results of the topology optimization problem with the combined approach using continuation and a volume fraction of 20% with a projection radius of $r_{min} = 3$ are shown in Fig. 29b. Similar to the previous example, the thick areas of material are no longer

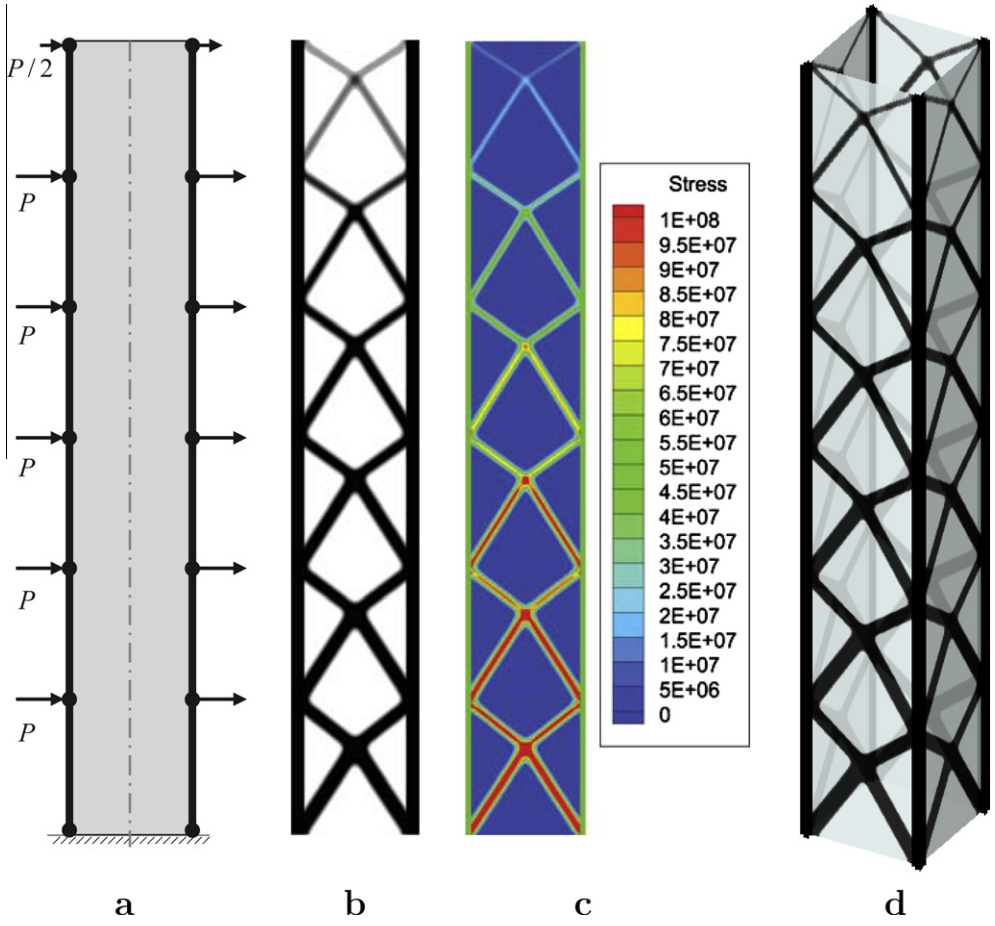

Fig. 29. Topology optimization for braced frame: (a) problem statement, (b) two-dimensional result, (c) stress distribution, and (d) three-dimensional rendering of result.

concentrated at the edges of the domain and the braces are complete and clearly defined. One interesting feature of this result shows the densities increase for the bracing members as the load increases throughout the height indicating that the sizes of the final members should increase accordingly. The Von Mises stresses for this geometry featuring modules of the same height are plotted in Fig. 29c, which are not constant throughout the structure due to the increasing densities along the height. In Fig. 29d a three-dimensional rendering of this result is given to show how these findings might be used to design a high-rise building.

8. Concluding remarks

The methodology presented in this work for developing a lateral braced frame system in a high-rise building enables the structural engineer to quickly and efficiently identify the optimal diagonal layout. In summary, the main contributions of this work are as follows:

- Several methodologies to connect discrete and continuum elements were explored.
- A technique was proposed for the design of an optimal braced frame system.
- The constant state of stress in an optimized frame under certain conditions was verified.
- The relevance of this new methodology in the context of high-rise building mechanics was demonstrated.
- The optimal geometry for a braced frame was analytically derived and numerically confirmed.

As an extension of the work presented in this paper, the use of shell elements with three-dimensional beam elements for large structural systems is currently under exploration by the authors.

Acknowledgment

The first author gratefully acknowledges the support from the National Science Foundation Graduate Research Fellowship Program (GRFP).

References

[1] Stromberg LL, Beghini A, Baker WF, Paulino GH. Application of layout and topology optimization using pattern gradation for the conceptual design of buildings. Struct Multidisc Optim 2011;43(2):165–80.
[2] Allahdadian S, Boroomand B. Design and retrofitting of structures under transient dynamic loads by a topology optimization scheme. In: Proc 3rd Int Conf Seism Retrofit, October, 2010. p. 1–9.
[3] Neves MM, Rodrigues H, Guedes JM. Generalized topology design of structures with a buckling load criterion. Struct Multidisc Optim 1995;10(2):71–8.
[4] Huang X, Xie YM. Topology optimization of nonlinear structures under displacement loading. Eng Struct 2008;30(7):2057–68.
[5] Huang C, Han X, Wang C, Ji J, Li W. Parametric analysis and simplified calculating method for diagonal grid structural system. Jianzhu Jiegou Xuebao/J Build Struct 2010;31(1):70–7.
[6] Prager W. Optimal layout of trusses with finite number of joints. J Mech Phys Solids 1978;26(4):241–50.
[7] Prager W. Nearly optimal design of trusses. Comput Struct 1978;8(3–4):451–4.
[8] Michell AGM. The limits of economy of material in frame-structures. Phil Mag 1904;8(47):589–97.
[9] Ben-Tal A, Nemirovski A. Robust optimization G methodology and applications. Math Program 2002;92(3):453.
[10] Mazurek A, Baker WF, Tort C. Geometrical aspects of optimum truss like structures. Struct Multidisc Optim 2011;43(2):231–42.

[11] Bendsoe M, Kikuchi N. Generating optimal topologies in structural design using a homogenization method. Comput Methods Appl Mech Eng 1988;71(2):197–224.
[12] Bendsoe M. Optimal shape design as a material distribution problem. Struct Optim 1989;1(4):193–202.
[13] Bendsoe M, Sigmund O. Topology optimization: theory, methods and applications. Springer; 2002.
[14] Takezawa A, Nishiwaki S, Izui K, Yoshimura M. Structural optimization based on topology optimization techniques using frame elements considering cross-sectional properties. Struct Multidisc Optim 2006;34(1):41–60.
[15] Fredricson H. Topology optimization of frame structures—joint penalty and material selection. Struct Multidisc Optim 2005;30(3):193–200.
[16] Kaveh A, Shahrouzi M. Graph theoretical topology control in structural optimization of frames with bracing systems. Sci Iran 2009;16(2):173–87.
[17] Wang D. Optimal shape design of a frame structure for minimization of maximum bending moment. Eng Struct 2007;29(8):1824–32.
[18] Diaz AR, Kikuchi N. Solutions to shape and topology eigenvalue optimization problems using a homogenization method. Int J Numer Method Eng 1992;35(7):1487–502.
[19] Liang QQ. Effects of continuum design domains on optimal bracing systems for multistory steel building frameworks. In: Proc 5th Australas Congr Appl Mech; vol. 2. Engineers Australia; 2007. p. 794–9.
[20] Liang QQ, Xie YM, Steven GP. Optimal topology design of bracing systems for multi-story steel frames. J Struct Eng – ASCE 2000;126(7):823–9.
[21] Mijar AR, Swan CC, Arora JS, Kosaka I. Continuum topology optimization for concept design of frame bracing systems. J Struct Eng – ASCE 1998;124(5):541–50.
[22] Lagaros N, Psarras L, Papadrakakis M, Panagiotou G. Optimum design of steel structures with web openings. Eng Struct 2008;30(9):2528–37.
[23] Baker WF. Energy-based design of lateral systems. Struct Eng Int 1992;2:99–102.
[24] Hill R. The mathematical theory of plasticity. New York: Oxford University Press Inc; 1950.
[25] Lubliner J. Plasticity theory. New York: Macmillan Publishing Company; 1990.
[26] Hemp W. Optimum structures. Oxford: Clarendon Press; 1973.
[27] Cook RD, Malkus DS, Plesha ME, Witt RJ. Concepts and applications of finite element analysis. 4th ed. Wiley; 2001. ISBN 0471356050.
[28] Kohn RV, Strang G. Optimal-design and relaxation of variational problems I. Commun Pure Appl Math 1986;39(1):113–37.
[29] Kohn RV, Strang G. Optimal-design and relaxation of variational problems II. Commun Pure Appl Math 1986;39(2):139–82.
[30] Petersson J, Sigmund O. Slope constrained topology optimization. Int J Numer Method Eng 1998;41(8):1417–34.
[31] Zhou M, Rozvany GIN. The COC algorithm. Part II: Topological, geometrical and generalized shape optimization. Comput Methods Appl Mech Eng 1991;89(1–3):309–36.
[32] Rozvany GIN, Zhou M, Birker T. Generalized shape optimization without homogenization. Struct Multidisc Optim 1992;4(3):250–2.
[33] Bendsoe M, Sigmund O. Material interpolation schemes in topology optimization. Arch Appl Mech 1999;69(9-10):635–54.
[34] Stolpe M, Svanberg K. An alternative interpolation scheme for minimum compliance topology optimization. Struct Multidisc Optim 2001;22(2):116–24.
[35] Guest JK, Prévost JH, Belytschko T. Achieving minimum length scale in topology optimization using nodal design variables and projection functions. Int J Numer Method Eng 2004;61(2):238–54.
[36] Sigmund O. A 99 line topology optimization code written in Matlab. Struct Multidisc Optim 2001;21(2):120–7.